energies

MDPI

Article

# Thermo-Economic Analysis of a Bottoming Kalina Cycle for Internal Combustion Engine Exhaust Heat Recovery

**Hong Gao * and Fuxiang Chen**

Key Laboratory of Low-Grade Energy Utilization Technologies and Systems of Ministry of Education, College of Power Engineering, Chongqing University, Chongqing 400030, China; 20161013088@cqu.edu.cn
* Correspondence: gaohong@cqu.edu.cn

Received: 28 September 2018; Accepted: 31 October 2018; Published: 6 November 2018

check for updates

**Abstract:** The use of a Kalina cycle (KC) with a superheater to recover waste heat from an internal combustion engine (ICE) is described in this paper. The thermodynamic and economic analyses are performed for KC. The results indicate that using KC with a superheater is a feasible method to recover waste heat from ICE. The maximum thermal efficiency of KC is 46.94% at 100% ICE percentage load. The improvement of thermal efficiency is greater than 10% at all ICE loads, and the maximum improvement of thermal efficiency is 21.6% at 100% ICE load. Both the net power output and thermal efficiency of the KC subsystem increase with ICE percentage load and ammonia mass fraction. A lower turbine inlet pressure leads to a higher net power output of KC and a greater improvement of thermal efficiency when the ammonia mass fraction of the mixture is greater than 0.34. In the paper, if the same KC, which uses the largest capital investment, is used at different ICE loads, the payback period decreases with ICE load and ammonia mass fraction. In addition, both longer annual operation times and lower interest rates lead to shorter payback periods. However, it is worth noting that the payback period will be longer than the ICE's lifetime if the ICE load is low and the annual operation time is too short.

**Keywords:** Kalina cycle; waste heat recovery; power output; thermal efficiency; payback period

---

## 1. Introduction

The internal combustion engine (ICE) is an important energy conversion device commonly used in automobiles, trucks, buses and ships. Though engine manufacturers have used all kinds of techniques or methods to improve thermal efficiency, approximately 60–70% of the fuel energy is taken away through coolant or exhaust. Due to the issues of energy shortage and environmental pollution, energy saving has become increasingly important. It is a feasible way to recover waste heat from ICE without increasing fuel consumption or emissions. Organic Rankine cycle (ORC) and KC are two feasible methods to recover waste heat. Because of its simplicity and adaptability for recovering waste heat at medium and low temperature, a majority of studies choose ORC for waste heat recovery. Wei et al. [1] concluded that the supercritical Rankine cycle is a suitable way to recover waste heat from a heavy-duty diesel ICE. Zhu et al. [2] analyzed the thermodynamic processes of a bottoming Rankine cycle for recovering engine waste heat and investigated the system exergy destruction with an exergy distribution map. Kostowski et al. [3] compared the ICE–ORC system with alternative throttling or expansion strategies based on a case study example. Seyedkavoosi et al. [4] proposed a novel two-parallel-step ORC for recovering waste heat from an ICE and performed an exergy analysis. Wang et al. [5] revealed that the engine working condition affects ORC dynamic response for a natural gas ICE with an ORC as the bottoming cycle. Pili et al. [6] used an ORC as the bottoming cycle to recover more than 6 kW of mechanical power from long-haul trucks waste heat, but the system would be very heavy and large. Wang et al. [7] proposed a dual-loop ORC system with R1233zd and R1234fy as the working fluid and found that this system could get better performance for similar applications than other ORC systems. Scaccabarozzi et al. [8] showed that a supercritical ORC using the optimal mixture has better thermal performance for heat recovery from heavy duty ICEs. Liu et al. [9] found that both the exergy efficiency and thermal efficiency of the MC/ORC system decreases linearly with the reduction of engine load. Wang et al. [10] illustrated that Double loop ORC (DORC) can increase the efficiency of the combined system by 12% at 60–100% engine load.

In addition to ORC, KC also shows good thermal performance for waste heat recovery due to its thermal match in heat exchangers during the heat transfer processes. Since Kalina [11] introduced KC using an ammonia-water mixture as the working fluid, many studies have been performed on KC. When KC was used as a bottoming cycle in combined cycle power plants, the thermal efficiency of KC was 30–60% higher than that of the Rankine cycle [12]; Fu et al. [13] found that compared to several other power cycles, using KC leads to an effectiveness enhancement of approximately 20% [13]. Hettiarachchi et al. [14] compared the performance of ORC and Kalina cycle system 11 (KCS11) for recovering low-temperature geothermal heat resources. They found that KCS11 has a better overall thermal performance at moderate pressures than that of ORC. Singh et al. [15] used a KC as the bottoming cycle to recover the waste heat from a coal-fired steam power plant. They found that there is an optimal ammonia mass fraction that produces the maximum cycle efficiency for a given turbine inlet pressure. Li et al. [16] found KC has better thermo-economic performance than that of the $CO_2$ transcritical power cycle by using low-temperature geothermal water as their heat resources. Yari et al. [17] compared the thermodynamic and economic performance of KCS11, ORC and the trilateral power cycle (TLC) and found that the net power from TLC is higher than that of KCS11 and ORC. Wang et al. [18] analyzed a composition-adjustable KC and found that the composition adjustment can improve system performance significantly. Fallah et al. [19] found that KC has high potential for efficiency improvement. Nemati et al. [20] concluded that ORC has significant advantages over KC for waste heat recovery from CGAM cogeneration system. Gharde et al. [21] believed that KC would be suitable for waste heat recovery for its high thermal efficiency and designed a KC subsystem to recover waste heat from a 1196 cc multi-cylinder petrol engine. Yue et al. [22] found that the transcritical ORC has higher overall thermal efficiency than that of KC for waste heat recovery under various different ICE working conditions.

In brief, a review of the published literatures indicates that both ORC and KC have promising thermal performance for recovering low- and moderate-temperature waste heat. However, few investigations focused on the thermodynamic and economic analyses of a bottoming KC for waste heat recovery from ICE. The ICE-Kalina system, composed of a topping ICE and a bottoming KC with a superheater, is proposed in this paper to recover waste heat from ICE. The thermodynamic and economic analyses are conducted for bottoming KC. The effects of several important parameters on thermal and economic performance, such as ICE percentage load and ammonia mass fraction, are investigated.

## 2. System Description and Assumptions

A schematic diagram of bottoming KC with a superheater for ICE waste heat recovery is shown in Figure 1. The waste heat of ICE is the heat source of bottoming KC. The working fluid of KC is an ammonia-water mixture. The main components of KC are evaporator, separator, superheater, low-temperature recuperator and high-temperature recuperator, turbine, condenser, and pump.

The ammonia-water mixture is heated in the evaporator (state 5), and then is separated into a saturated ammonia-water vapor (state 6) and an ammonia-water liquid (state 9) in the separator. After the separator, the separated ammonia-water vapor goes into the superheater to increase its temperature. Next, the vapor passes through the turbine (state 8) to generate power. Saturated ammonia-water liquid (state 9), after absorbing some heat in the high-temperature recuperator (state 10), is throttled down to a low pressure (state 11) and mixed with the ammonia-water vapor leaving the turbine in the mix tank (state 12). After that step, the ammonia-water mixture enters the low-temperature recuperator to preheat the ammonia-water solution at its cold side. Next, the ammonia-water mixture (state 13) releases heat in the condenser and increases pressure through the pump (state 15). Then the ammonia-water mixture flows to the evaporator via the low- and high-temperature recuperators, sequentially.

If $T_1$ is low, the ammonia-water vapor (state 6) will go to the turbine through bypass 1 instead of flowing through the superheater. When $T_9$ is lower than $T_4$, the working fluids at state 9 and state 16 will not flow through the high-temperature recuperator and will go to the valve and the evaporator through bypasses 2 and 3, respectively.

The following assumptions are used in this work:

1. The KC subsystem does not influence the operation condition of ICE.
2. The KC system operates in a steady-state.
3. Changes in kinetic and potential energies are negligible.
4. The pressure loss due to frictional effects is negligible.
5. The ammonia-water mixture leaving the condenser (state 14) is a saturated liquid.
6. The minimum pinch-point temperature difference of all heat exchangers is 10K.

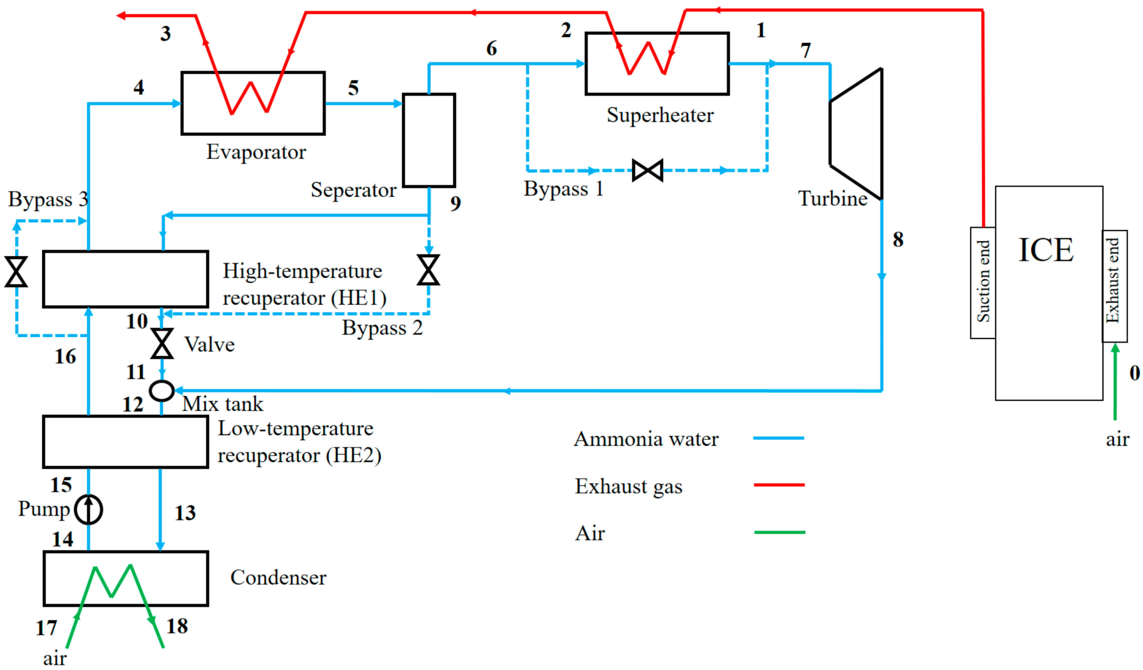


**Figure 1.** Schematic of bottoming KC with a superheater for ICE waste heat recovery.

## 3. System Modeling

### *3.1. Thermodynamic Modeling*

For thermodynamic analysis, the principles of mass and energy conservations are applied to each component. The energy relations for the equipment of the ICE-Kalina system are listed in Table 1.

**Table 1.** Energy relations for equipment of the ICE-Kalina system.

| Subsystem | Equipment | Energy Equations |
|---|---|---|
| The topping ICE system | | $Q_0 = P_{ICE} + Q_{loss} + Q_1 + Q_2$<br>$Q_3 = m_1 c_p (T_1 - T_3) = Q_{eva} + Q_{sup}$ |

**Table 1.** *Cont.*

| Subsystem | Equipment | Energy Equations |
|---|---|---|
| The bottoming Kalina cycle | Evaporator | $Q_{eva} = m_4(h_5 - h_4) = m_1(h_2 - h_3)$ |
| | Superheater | $Q_{sup} = m_6(h_7 - h_6) = m_1(h_1 - h_2)$ |
| | Separator | $m_9h_9 + m_6h_6 = m_4h_5$ |
| | HE1 | $m_9(h_9 - h_{10}) = m_4(h_4 - h_{16})$ |
| | HE2 | $m_9(h_{12} - h_{13}) = m_4(h_{16} - h_{15})$ |
| | Condenser | $Q_{con} = m_9h_{13} - m_4h_{14}$ |
| | Turbine | $W_T = m_6(h_7 - h_{8,s})\eta_{s,T}$ |
| | Pump | $W_p = m_4(h_{15,s} - h_{14})/\eta_{s,p}$ |
| | Throttle valve | $h_{10} = h_{11}$ |
| | Mix tank | $m_9h_{11} + m_6h_8 = m_4h_{12}$ |

$Q_0$ is the overall fuel heating value during combustion. $Q_1$ is the cooling heat taken away by the coolant and lubricant. $Q_2$ is the waste heat of the exhaust exiting the ICE. $Q_{loss}$ is the heat loss of the engine thermodynamic cycle. $P_{ICE}$ is the net power output of the ICE system. $Q_3$ is the waste heat recovered by bottoming KC [22]. $\eta_{s,T}$ and $\eta_{s,P}$ represent the isentropic efficiencies of the turbine and the pump, respectively; both are 0.85 in this paper.

The net power output of the ICE-Kalina system, including the net power outputs of ICE and KC, can be defined as follows:

$$W_{net} = P_{ICE} + W_{net,Kalina} \tag{1}$$

The overall thermal efficiency of the ICE-Kalina system is defined as follows:

$$\eta_t = \frac{P_{ICE} + W_{net,Kalina}}{Q_0} \tag{2}$$

Thermal efficiency of the topping ICE subsystem is calculated by:

$$\eta_{t\_ICE} = \frac{P_{ICE}}{Q_0} \tag{3}$$

Improvement of the thermal efficiency is calculated by:

$$\Delta\eta_t = \frac{\eta_t - \eta_{t\_ICE}}{\eta_{t\_ICE}} \tag{4}$$

The exergetic efficiency of the evaporator in KC is defined by:

$$\eta_{ex\_evp} = \frac{E_{x5} - E_{x4}}{E_{x2} - E_{x3}} \tag{5}$$

The exergetic efficiency of the superheater in KC is defined by:

$$\eta_{ex\_sup} = \frac{E_{x7} - E_{x6}}{E_{x1} - E_{x2}} \tag{6}$$

The exergetic efficiency of KC is defined by:

$$\eta_{ex\_Kalina} = \frac{W_{net\_Kalina}}{E_{x1} - E_{x3}} \tag{7}$$

Verification of Ammonia-Water Thermodynamic Properties

A MATLAB (R2014a, MathWorks, Natick, MA, USA) code has been developed to conduct the numerical simulations for the ICE-Kalina system. The thermodynamic properties of the ICE exhaust gas are evaluated by REFPROP (Version 9.0, National Institute of Standards and Technology (NIST), CO, USA) The thermodynamic properties of the KC states are evaluated by the method proposed by Xu and Goswami [23].

To verify the thermodynamic models for KC in the paper, data available in the published literature are used. The numerical models have been validated using data from Ref. [22] under the same operating conditions. Comparisons between the simulation results and those from Ref. [22] are presented in Table 2. The data in Table 2 shows a little difference between the simulation results of this paper and those in Ref. [22]. This is because the thermodynamic properties in Ref. [22] are simulated via the simulation platform of Aspen Plus, and the thermodynamic properties of ammonia-water mixture in this paper are evaluated by the method proposed by Ref. [23]. The thermal efficiency of KC in Ref. [22] is 18.8%, and the efficiency of KC without the superheater in this paper is 19.4%. Therefore, the data in Table 2 still indicate a good agreement between the simulation results of this paper and those in the published literature.

**Table 2.** Validation of the numerical model with the published data.

| Parameter | Pressure/bar | | Temperature/K | | Mass Rate/m$^3$/kg | | Ammonia Mass Fraction | |
|---|---|---|---|---|---|---|---|---|
| No. | Simulation | Ref. [22] | Simulation | Ref. [22] | Simulation | Ref. [22] | Simulation | Ref. [22] |
| 4 | 53 | 53 | 437 | 433 | 2.07 | 2.06 | 0.37 | 0.37 |
| 5 | 53 | 53 | 494 | 494 | 2.07 | 2.06 | 0.37 | 0.37 |
| 6 | 53 | 53 | 494 | 494 | 0.71 | 0.668 | 0.584 | 0.616 |
| 8 | 3.97 | 3.97 | 382 | 381 | 0.71 | 0.668 | 0.584 | 0.616 |
| 9 | 53 | 53 | 494 | 494 | 1.36 | 1.39 | 0.247 | 0.252 |
| 10 | 53 | 53 | 388 | 380 | 1.36 | 1.39 | 0.247 | 0.252 |
| 11 | 3.97 | 3.97 | 352 | 345 | 1.36 | 1.39 | 0.247 | 0.252 |
| 13 | 3.97 | 3.97 | 337 | 334 | 2.07 | 2.06 | 0.37 | 0.37 |
| 14 | 3.97 | 3.97 | 301 | 301 | 2.07 | 2.06 | 0.37 | 0.37 |
| 15 | 53 | 53 | 302 | 302 | 2.07 | 2.06 | 0.37 | 0.37 |

### 3.2. Economic Modeling

To evaluate the thermo-economic performance of the Kalina subsystem, the payback period for KC is analyzed in this paper.

It is necessary to get the total capital cost of KC to calculate the payback period. According to Ref. [24], the heat exchangers, pump and turbine contribute largely to the total cost. This finding is reasonable because 80–90% of the capital cost of the system is attributed to heat exchangers [25]. We assume that all of the heat exchangers in the KC system are shell-and-tube heat exchangers [26,27].

The total heat transfer rate per unit time, can be calculated by [28]:

$$Q = UA\Delta T_m = UA\left[\frac{(\Delta T_{\max} - \Delta T_{\min})}{\ln(\Delta T_{\max}/\Delta T_{\min})}\right] \tag{8}$$

It is tedious to determine the overall heat transfer coefficient $U$, and the data needed in this instance are not available at the preliminary stages of the design. Therefore, for preliminary calculations, as a first approximation, the values of the overall heat transfer coefficient are given in Table 3 [29].

**Table 3.** Overall heat transfer coefficients for heat exchangers [29].

| Component | Overall Heat Transfer Coefficient (W/m$^2$K) |
|---|---|
| Evaporator | 1100 |
| Conderser | 500 |
| Superheater | 300 |
| Recuperator | 700 |

The equipment module costing method is used to evaluate the equipment costs. Considering the impact of inflation, the Chemical Engineering Plant Cost Index (CEPCI) is used to convert the total equipment cost of the system at the base time into that of the year of 2017 [30], which is expressed as:

$$C_{2017} = C_b\left(\frac{I_{2017}}{I_b}\right) \tag{9}$$

where $C_b$ is the cost at the base time, and $I_{2017}$ and $I_b$ are the cost indices assigned 567.5 [31] and 397 [30], respectively.

If the equipments are made of carbon-steel and operate at ambient pressures, the purchased cost of the equipment can be calculated by [30]:

$$\mathrm{lg}C_{eq}^0 = K_1 + K_2\mathrm{lg}Z + K_3(\mathrm{lg}Z)^2 \tag{10}$$

where $C_{eq}^0$ is the purchased cost of the equipment at ambient pressures using carbon steel construction and $Z$ is the capacity of the equipment. For the heat exchanger, $Z$ refers to the area of heat exchange $A$. For the pump, $Z$ refers to the power consumption of the pump, $W_p$. For the turbine, $Z$ represents the power output, $W_T$. For the separator, $Z$ represents the volume of the separator, $V_{sep}$. The coefficients of $K_1$, $K_2$ and $K_3$, are listed in Table 4.

Assuming each heat exchanger of the system is a carbon-steel shell-and-tube heat exchanger, the cost is given by [30]:

$$C_{he} = \frac{567.5}{397}C_{he}^0\left(B_{1,he} + B_{2,he}F_{M,he}F_{p,he}\right) \tag{11}$$

where $B_{1,he}$ and $B_{2,he}$ are constants based on the type of heat exchanger, $F_{M,he}$ is the material factor and $F_{P,he}$ is the pressure factor, which is calculated as [30]:

$$lgF_{p,he} = C_{1,he} + C_{2,he}lgp_{he} + C_{3,he}(lgp_{he})^2 \tag{12}$$

where $C_{1,he}$, $C_{2,he}$ and $C_{3,he}$ are constants in terms of the type and pressure range of the heat exchanger.

The turbines in this work are made of carbon steel with axial types; their costs are calculated as [30]:

$$C_{turb} = \frac{567.5}{397}C_{turb}^0F_{BM,turb} \tag{13}$$

where $F_{BM,turb}$ refers to the bare module factor according to the type and material of construction of the turbine.

For the separator, carbon steel and vertical type are chosen for construction. The cost is expressed as [30]:

$$C_{sep} = \frac{567.5}{397}C_{sep}^0(B_{1,sep} + B_{2,sep}F_{M,sep}F_{p,sep}) \tag{14}$$

where $B_{1,sep}$ and $B_{2,sep}$ are constants according to the type of separator, $F_{M,sep}$ is the material factor and $F_{p,sep}$ is the pressure factor, which is calculated by [30]:

$$F_{p,sep} = \max\left\{\frac{\frac{(p_{sep}+1)\cdot D_{sep}}{2\cdot[850-0.6\cdot(p_{sep}+1)]} + 0.00315}{0.0063}, 1\right\} \tag{15}$$

The pumps are centrifugal and made from stainless steel; their costs are given by [30]:

$$C_{pump} = \frac{567.5}{397}C_{pump}^0(B_{1,pump} + B_{2,pump}F_{M,pump}F_{p,pump}) \tag{16}$$

where $B_{1,pump}$ and $B_{2,pump}$ are constants in terms of the type of the pump, $F_{M,pump}$ is the material factor and $F_{P,pump}$ is the pressure factor, which is given by [30]:

$$lgF_{p,pump} = C_{1,pump} + C_{2,pump}lgp_{pump} + C_{3,pump}\left(lgp_{pump}\right)^2 \quad (17)$$

where $C_{1,pump}$, $C_{2,pump}$ and $C_{3,pump}$ are constants according to the type and pressure range of the pump.

The constants mentioned above are all listed in Table 4.

**Table 4.** Constants for equipment costs calculation [30].

| Constant | Value | Constant | Value | Constant | Value |
|---|---|---|---|---|---|
| $K_{1,he}$ | 4.3247 | $K_{2,pump}$ | 0.0536 | $C_{2,he}$ | 0.11272 |
| $K_{2,he}$ | −0.303 | $K_{3,pump}$ | 0.1538 | $C_{3,he}$ | 0.08183 |
| $K_{3,he}$ | 0.1634 | $B_{1,he}$ | 1.63 | $C_{1,pump}$ | −0.3935 |
| $K_{1,turb}$ | 2.7051 | $B_{2,he}$ | 1.66 | $C_{2,pump}$ | 0.3957 |
| $K_{2,turb}$ | 1.4398 | $B_{1,sup}$ | 2.25 | $C_{3,pump}$ | −0.00226 |
| $K_{1,sup}$ | 3.4974 | $B_{2,sup}$ | 1.82 | $F_{M,he}$ | 1 |
| $K_{2,sup}$ | 0.4485 | $B_{1,pump}$ | 1.89 | $F_{BM,turb}$ | 3.5 |
| $K_{3,sup}$ | 3.4974 | $B_{2,pump}$ | 1.35 | $F_{M,sep}$ | 1 |
| $K_{1,pump}$ | 3.3892 | $C_{1,he}$ | 0.03881 | $F_{M,pump}$ | 2.2 |

The capital recovery factor ($CRF$) is defined as follows [30]:

$$CRF = \frac{i(1+i)^{T_s}}{(1+i)^{T_s} - 1} \quad (18)$$

where $i$ is the interest rate (4.3%) [32,33]. The economic lifetime of the ICE-Kalina system ($T_s$) is 15 years [32]. The payback period is given by:

$$\left(W_{net\_Kalina} \cdot OP_s \cdot C_{pri} - COM_s\right) \cdot \left(\frac{(1+i)^{\tau} - 1}{i \cdot (1+i)^{\tau}}\right) = C_{2017} \quad (19)$$

Next, the payback period of the system is evaluated by Equation (19) [33]:

$$\tau \approx \frac{C_{2017}}{\left(W_{net\_Kalina} \cdot OP_s \cdot C_{pri} - COM_s\right) \cdot (1-i)} \quad (20)$$

where $C_{pri}$ is the price of electricity (the price of electricity in China in 2017 is approximately 0.63 yuan/kWh, which is 0.1 $/kWh based on the ratio of RMB to USD) [34]. $OP_s$ is the annual operation time, which changes from 3700 to 8500 h in the paper. $COM_s$ is the system operational and maintenance costs (1.65% of $C_{2017}$) [35].

The Kalina subsystem used for ICE waste heat recovery can reduce the fossil fuel consumption and $CO_2$ emission. If KC is used instead of a petroleum-fired power plant, the annual saved petroleum $M_{pe}$ (kL/year) and reduced $CO_2$ emission $M_{em}$ (kg/year) can be estimated as [36]:

$$M_{pe} = OP_s \cdot a_{pe} \cdot W_{net\_Kalina} \quad (21)$$

$$M_{em} = OP_s \cdot a_{em} \cdot W_{net\_Kalina} \quad (22)$$

where $a_{pe}$ is the amount of petroleum consumed to produce 1 kWh of electrical energy and $a_{em}$ is the amount of $CO_2$ emissions if 1 kWh of electrical energy is produced by a petroleum-fired power plant. The values are assumed as follows: $a_{pe}$ = 0.266 L/(kWh) and $a_{em}$ = 0.894 kg/(kWh) [36].

## 4. Results and Discussion

### 4.1. Thermal Performance Analysis for KCs

Table 5 gives the waste exhaust operation parameters at different ICE percentage loads for 3561CDITA ICE [22]. The thermodynamic performance of the proposed system at full load is calculated. Table 6 gives the parameters of some states in the Kalina subsystem at 100% ICE load.

The thermodynamic performance of the ICE-Kalina system is calculated and compared with Ref. [22], as illustrated in Table 6. The results show that the heat recovered from the ICE, the turbine work and the net power output of the ICE-Kalina system are 920 kW, 436.6 kW and 432 kW, respectively. The overall thermal efficiency of the ICE-Kalina system is 43.5%. Compared with the ICE system, the improvement of the thermal efficiency is 21.6%. The thermal efficiency of the proposed subsystem is much higher than the subsystem in Ref. [22]. This finding is observed because the KC with a superheater has a better thermal match in the heat transfer exchangers than the KC without a superheater in Ref. [22], especially at high exhaust inlet temperatures. This means that when the ICE load is high, the proposed Kalina subsystem with a superheater is more efficient than the Kalina subsystem in Ref. [22].

The Kalina subsystem could effectively reduce $CO_2$ emissions and petroleum consumption. Under the working conditions shown in Table 6, 503.2 kL of petroleum was saved and 1691 tons $CO_2$ was reduced per year. These data indicate that using the Kalina subsystem is an effective way to reduce the petroleum consumption and reduce the emission of $CO_2$.

**Table 5.** Waste exhaust parameters at different ICE loads [22] ($p_1$ = 101 kPa).

| ICE Load Percentage | Fuel Total Heating Value $Q_0$ (kW) | Power Output $P_{ICE}$ (kW) | Thermal Efficiency of ICE $\eta_{t\_ICE}$ (%) | Exhaust Gases Temperature $T_1$ (K) |
|---|---|---|---|---|
| 100 | 5590 | 2000 | 35.78 | 712 |
| 90 | 5050 | 1800 | 35.64 | 683 |
| 80 | 4560 | 1600 | 35.09 | 660 |
| 75 | 4330 | 1500 | 34.64 | 649 |
| 70 | 4110 | 1400 | 34.06 | 638 |
| 60 | 3640 | 1200 | 32.97 | 618 |
| 50 | 3120 | 1000 | 32.05 | 596 |
| 40 | 2580 | 800 | 31.01 | 569 |
| 30 | 2050 | 600 | 29.27 | 535 |
| 25 | 1810 | 500 | 27.62 | 514 |
| 20 | 1560 | 400 | 25.64 | 491 |
| 10 | 1060 | 200 | 18.87 | 419 |

**Table 6.** Primary thermodynamic performance indices of bottoming cycle.

| Items | Value | Value in Ref. [22] | Items | Value | Value in Ref. [22] |
|---|---|---|---|---|---|
| ICE load percentage (%) | 100% | 100% | $Q_3$ (kW) | 920 | 1151 |
| fuel total heating value $Q_0$ (kW) | 5590 | 5590 | $Q_4$ (kW) | 448 | 935 |
| power output $P_{ICE}$ (kW) | 2000 | 2000 | $W_{T\_Kalina}$ (kW) | 436.6 | 217 |
| exhaust gases volume flow rate ($m^3/s$) | 7.2 | 7.2 | $W_{net\_Kalina}$ (kW) | 432 | |
| exhaust gases temperature $T_1$ (K) | 712 | 712 | $\eta_{t\_kalina}$ (%) | 46.94 | 18.8 |
| turbine inlet temperature $T_7$ (K) | 692 | 494 | $\eta_{t\_ICE}$ (%) | 35.78 | 35.78 |
| turbine inlet pressure $p_7$ (bar) | 30 | 53 | $\Delta\eta_t$ (%) | 21.6 | 15.1 |
| ammonia mass fraction $x_4$ | 0.56 | 0.37 | payback period (year) | 2.94 | |
| $m_4$ (kg/s) | 0.985 | | $M_{em}$ (tons/year) | 1691 | |
| $m_6$ (kg/s) | 0.952 | | $M_{pe}$ (kL/year) | 503.2 | |

### 4.2. Thermal Performance

#### 4.2.1. Effect of the ICE Load

The ICE load is an extremely important operation parameter for the Kalina subsystem using the exhaust as its heat resource because it influences the temperature ($T_1$) and mass flow rate ($m_1$) of the exhaust gas. The temperature and mass flow rate of the exhaust gas increase with the ICE load. As shown in Figure 2, higher ICE percentage loads affect the turbine inlet temperature ($T_7$) and the mass flow rate of the ammonia-water vapor ($m_7$).

Figure 3 shows the effect of ICE percentage load on the exergy efficiency of the evaporator ($\eta_{ex\_evp}$), superheater ($\eta_{ex\_sup}$), and KC ($\eta_{ex\_Kalina}$). Both the exergy efficiencies of the evaporator and the superheater decrease first and then increase with ICE load and are greater than 80% at all ICE loads due to the good thermal match of the evaporator and the superheater. The exergy efficiency of the evaporator and the superheater reach their maximum values at 20% and 25% ICE load, respectively. The exergy efficiency of KC increases with ICE load. The increase of the exergy efficiency of KC becomes greater when the ICE load is greater than 60%. This is because the growth of $W_{net\_Kalina}$ is larger from 60% to 100% load, while the growth of ($E_{x1}-E_{x3}$) is smaller in this load range. The exergy efficiency of KC has its maximum value at 100% ICE load.

If the turbine outlet pressure is fixed, the enthalpy drop in the turbine increases with increasing turbine inlet temperature. Therefore, the net power output of both KC ($W_{net\_Kalina}$) and the ICE-Kalina system ($W_{net}$) increases as the ICE percentage load increases (Figure 4). As shown in Figure 5, the thermal efficiency of KC ($\eta_{t\_Kalina}$), the overall thermal efficiency of ICE-Kalina system ($\eta_t$) and the improvement of thermal efficiency of ICE ($\Delta\eta_t$) increase with ICE percentage load. When ICE percentage load is at 100% with a turbine inlet pressure of 30 bar and an ammonia mass fraction of 0.56, the improvement of thermal efficiency of ICE is 21.6%.

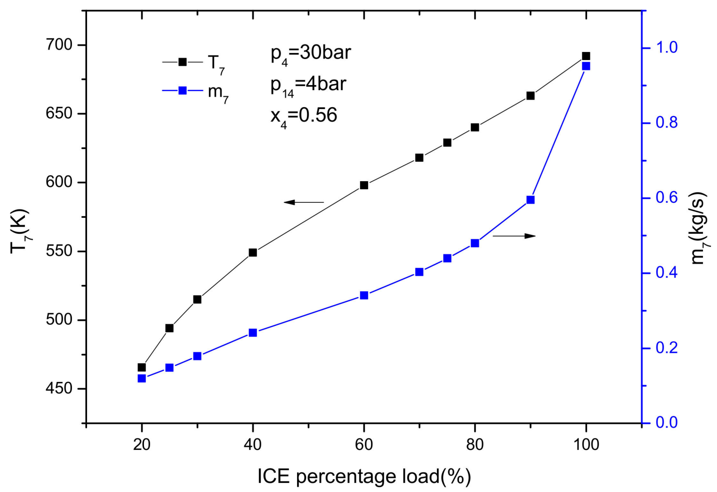


**Figure 2.** Effects of ICE percentage load on $T_7$ and $m_7$.

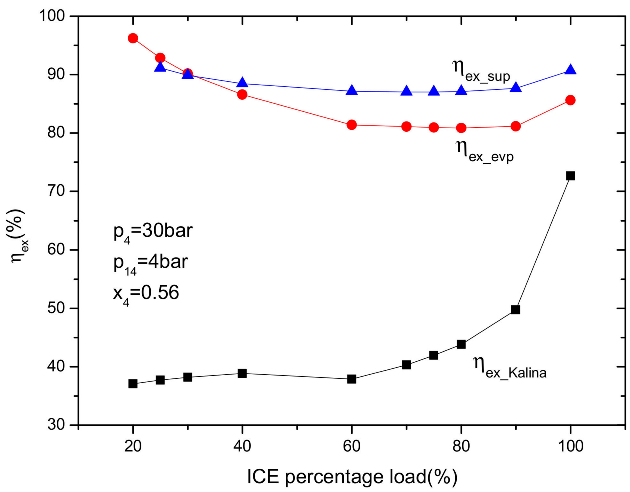


**Figure 3.** Effects of ICE percentage load on $\eta_{ex\_evp}$, $\eta_{ex\_sup}$ and $\eta_{ex\_Kalina}$.

Figure 6 shows the maximum value of the net power output of KC, the thermal efficiency of KC, the overall thermal efficiency of ICE-Kalina system, the improvement of thermal efficiency of ICE and the exergy efficiency of KC at different ICE loads. The optimal net power output of KC increases with the ICE load. The maximum thermal efficiency of KC increases first, has a maximum value at 90% ICE load and then later decreases. This effect is due to the greater increase of waste heat recovered by bottoming KC ($Q_3$) than that of the net power output of KC at 100% ICE load. Moreover, all values of the maximum improvement of thermal efficiency are greater than 10% at all ICE loads. The minimum improvement of thermal efficiency is 10.3% at 25% ICE load. This means that using KC with superheat is a feasible method to recover ICE waste heat. The maximum exergy efficiency of KC has a similar trend as maximum thermal efficiency and achieves its maximum value at 90% ICE load. According to the comparison, it is concluded that the maximum net power output and the thermal efficiency of KC in this paper are greater than those reported in Ref. [22] at all ICE loads, and the values of maximum exergy efficiency are greater than those in Ref. [22] when the ICE load is greater than 40%.

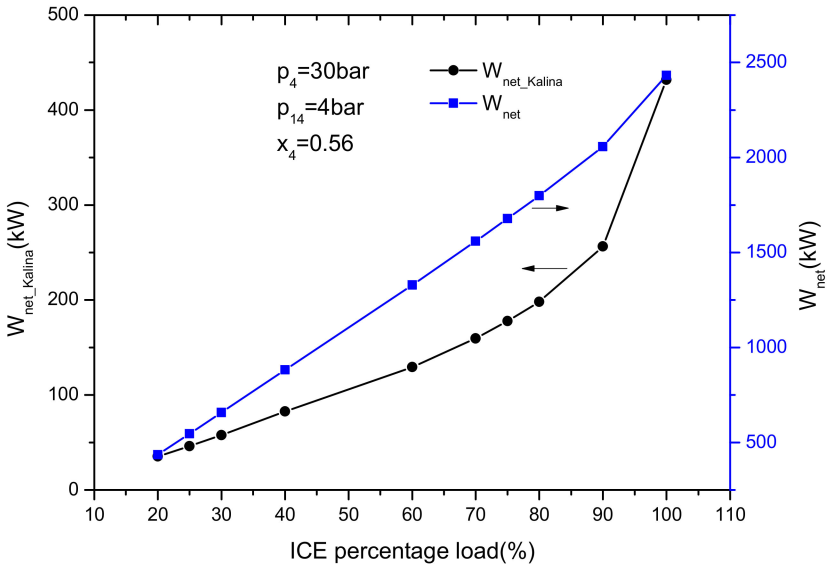


**Figure 4.** Effects of ICE percentage load on $W_{net\_Kalina}$ and $W_{net}$.

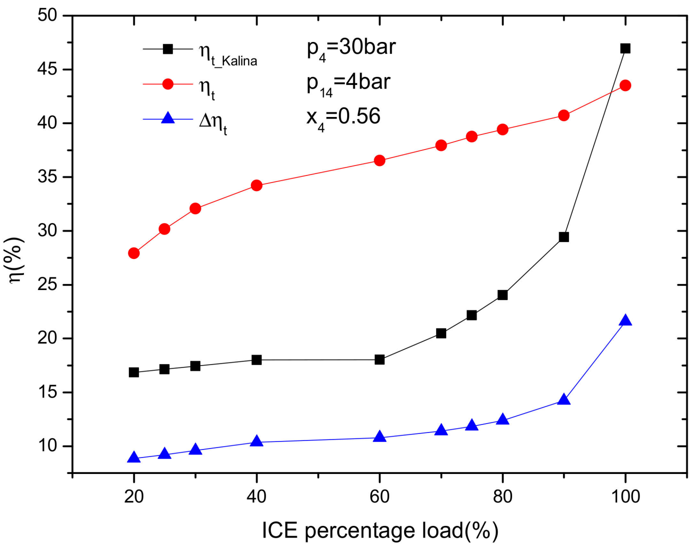


**Figure 5.** Effects of ICE percentage load on $\eta_{t\_Kalina}$, $\eta_t$ and $\Delta\eta_t$.

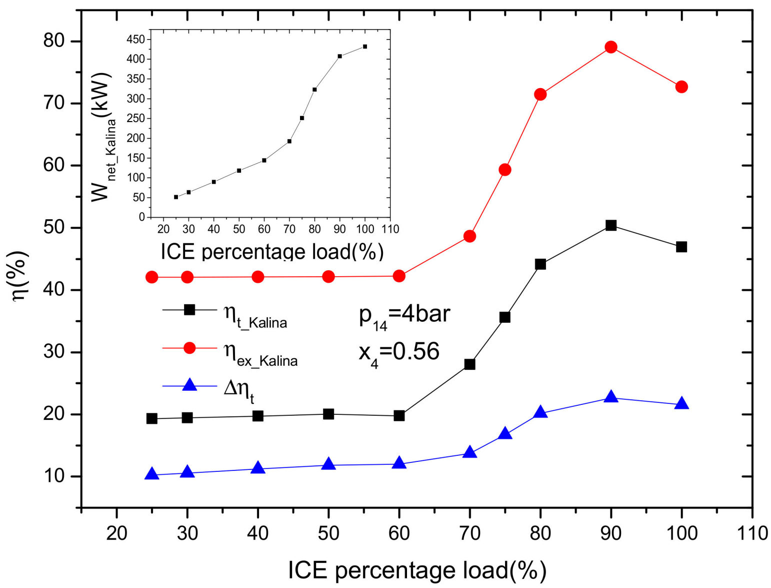


**Figure 6.** Maximum $\eta_{t\_Kalina}$, $\eta_t$, $\Delta\eta_t$ and $\eta_{ex\_Kalina}$ at different ICE percentage loads.

### 4.2.2. Effect of Turbine Inlet Pressure

As shown in Figure 7, the mass flow rate of the ammonia-water vapor ($m_7$) changes slightly with the turbine inlet pressure when the mass fraction of the ammonia-water mixture is 0.3. The mass flow rate of the ammonia-water vapor decreases and then increases with turbine inlet pressure when the ammonia mass fraction is 0.4 or 0.5. The enthalpy drop in the turbine increases as turbine inlet pressure increases. Therefore, the net power output of KC increases with an ammonia mass fraction of 0.3 and decreases and subsequently increases with an ammonia mass fraction of 0.4 or 0.5. As shown in Figure 8, the influence of turbine inlet pressure on KC thermal efficiency and the improvement of the thermal efficiency of ICE have similar tendencies with net power output. In short, within the simulation scope of this paper, if the ammonia mass fraction is below 0.34, higher turbine inlet pressures are better. If the ammonia mass fraction is greater than 0.34, a lower turbine inlet pressure is better.

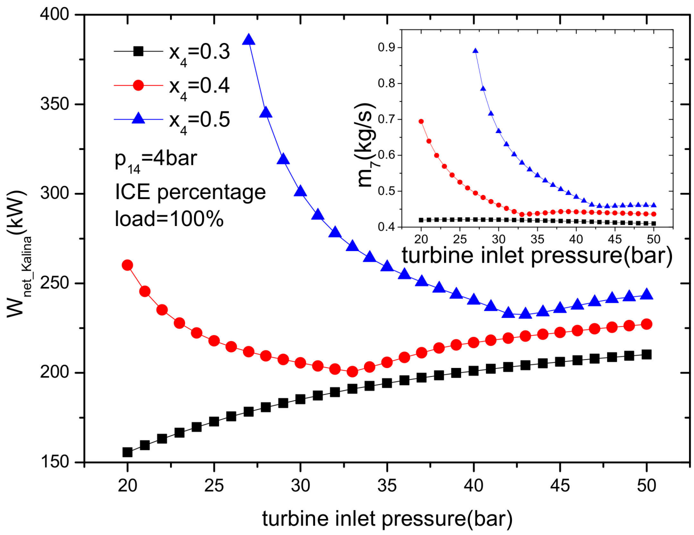


**Figure 7.** Effects of turbine inlet pressure on $W_{net\_Kalina}$.

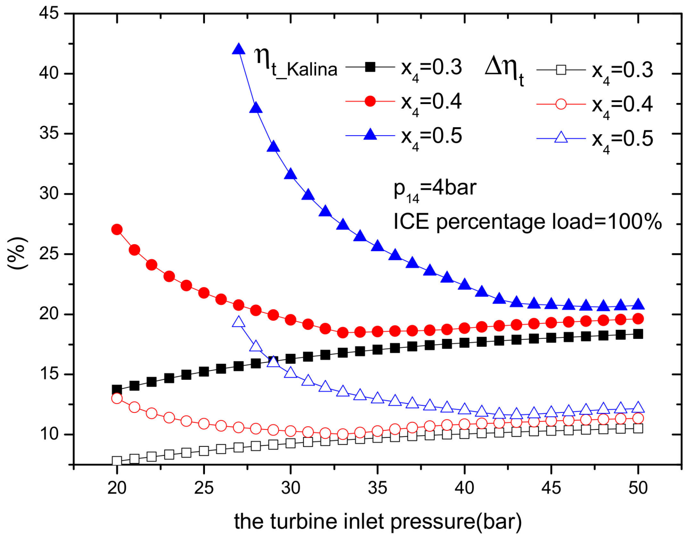


**Figure 8.** Effects of turbine inlet pressure on $\Delta\eta_t$.

### 4.2.3. Effect of Ammonia Mass Fraction

Figures 9 and 10 reveal that net power output, KC thermal efficiency and the improvement of the thermal efficiency of ICE benefit from an increased ammonia mass fraction. This finding is observed because the higher the ammonia mass fraction is, the greater the enthalpy drop of the vapor and the vapor flow rate expanding in the turbine is. The improvement of the thermal efficiency of ICE also increases with increased ammonia mass fraction. However, if the ammonia mass fraction is too high, the pump power consumption will increase greatly because the ammonia liquid mixture at the outlet of the condenser (state 14) will turn into a vapor–liquid mixture. This leads to great increase of the work consumption in the pump.

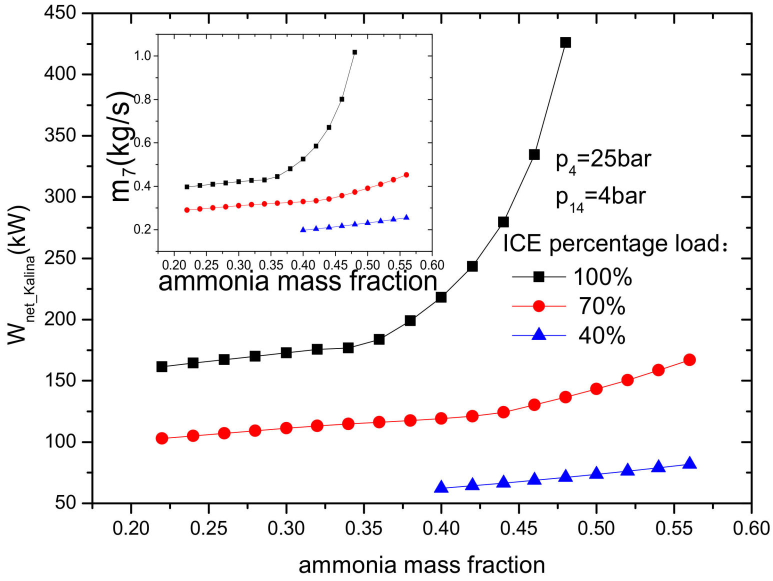


**Figure 9.** Effects of ammonia mass fraction on $W_{net\_Kalina}$.

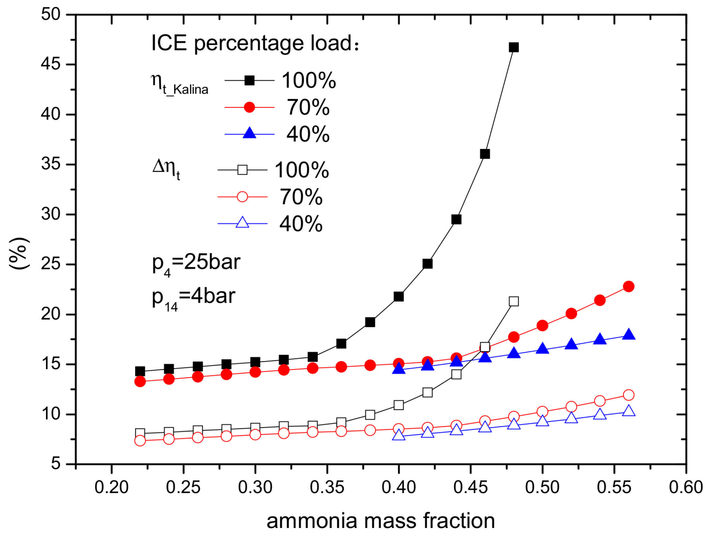


**Figure 10.** Effects of ammonia mass fraction on $\Delta\eta_t$.

*4.3. Economic Performance*

By increasing ICE load, the equipment capital investment increases due to a larger heat transfer area. Therefore, the Kalina subsystem has the largest capital investment $C_{2017}$ at 100% ICE load with an ammonia mass fraction of 0.56 and turbine inlet pressure of 30 bar. If the largest investment ($C_{2017}$) is taken as the investment of the Kalina subsystem at all loads, the effects of ICE load, turbine inlet pressure and ammonia mass fraction on the payback period are analyzed.

As shown in Figure 11, the minimum payback period decreases with ICE percentage load. This finding is observed because when the equipment investment remains fixed, a higher ICE load leads to more power output and a shorter payback period. The minimum payback periods are 2.44 years, 2.00 years, 1.69 years and 1.47 years at 100% ICE load with annual operation times of 4500 h, 5500 h, 6500 h and 7500 h, respectively. The maximum payback periods are 18.71 years, 15.59 years, 13.36 years and 11.69 years at 25% ICE load with annual operation times of 4500 h, 5500 h, 6500 h and 7500 h, respectively. The minimum payback period of the Kalina subsystem is shorter than the lifetime of 15 years when ICE percentage load is not below 30% and the annual operation times is not below

4500 h. This means that if ICE does not often runs at low loads, the Kalina subsystem can recover the capital investment over the lifetime of the equipment.

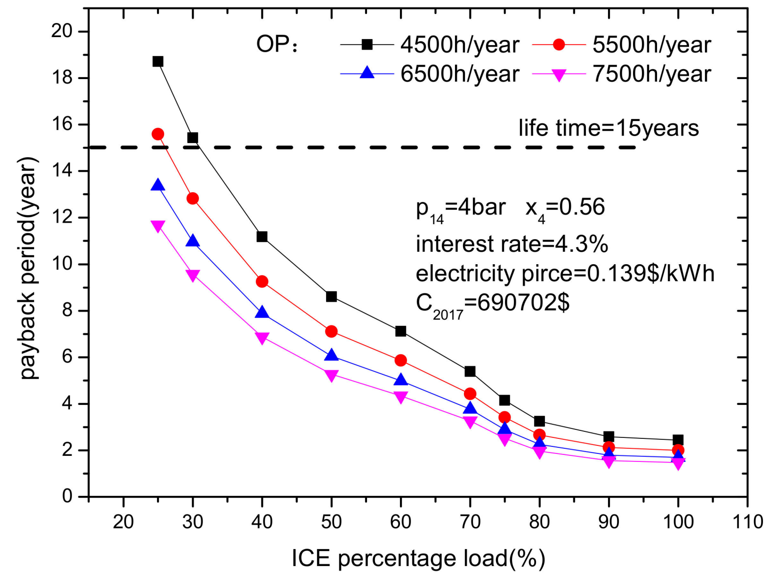


**Figure 11.** Minimum payback period at different ICE percentage loads.

The variations of payback period with turbine inlet pressure are presented in Figure 12. Payback period increases and later decreases with turbine inlet pressure if ICE load is not less than 60%. When ICE loads are 100% and 80%, the minimum payback periods are 1.69 years and 2.26 years, respectively, when the turbine inlet pressures are 30 bar and 20 bar, respectively. When ICE loads are 60% and 40%, the minimum payback periods are 5.20 years and 8.62 years, respectively, at a turbine inlet pressure of 50 bar. In short, if the ICE load is high, for example, not less than 70% with an ammonia mass fraction of 0.56, a lower turbine inlet pressure is better for reducing the payback period.

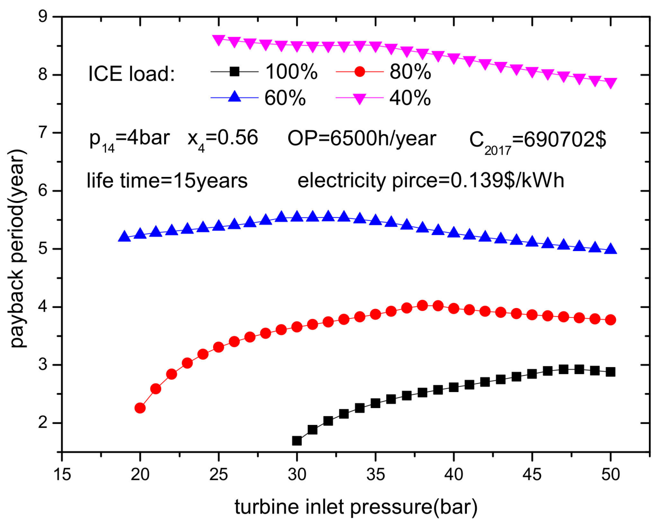


**Figure 12.** Effects of turbine inlet pressure on payback period.

Figure 13 shows that payback period decreases with ammonia mass fraction. This means that a high ammonia mass fraction is good for improving the economic performance of the Kalina subsystem. If the capital investment is fixed, a higher ammonia mass fraction will lead to higher net power output and a shorter payback period. When ICE load is 100%, 80%, 60% and 40%, the minimum payback periods are 1.72 years, 3.30 years, 5.38 years and 8.62 years, respectively.

Figure 14 shows the variation of payback period with annual operation time. Payback period decreases with increasing annual operation time. If annual operation time increases from 3700 h to 8500 h, the decrease of payback period is from 54% to 56% at all ICE loads. This means that annual operation time is a sensible and key parameter to estimate payback period. According to the calculation, payback period is less than 15 years when ICE load does not go below 40%. Figure 15 shows the influence of interest rate on payback period. Higher interest rates result in longer payback periods. When interest rate increases from 2.2% to 8%, the increase of the payback period is from 5.5% to 6%. This finding means that the influence of interest rate on payback period is relatively small.

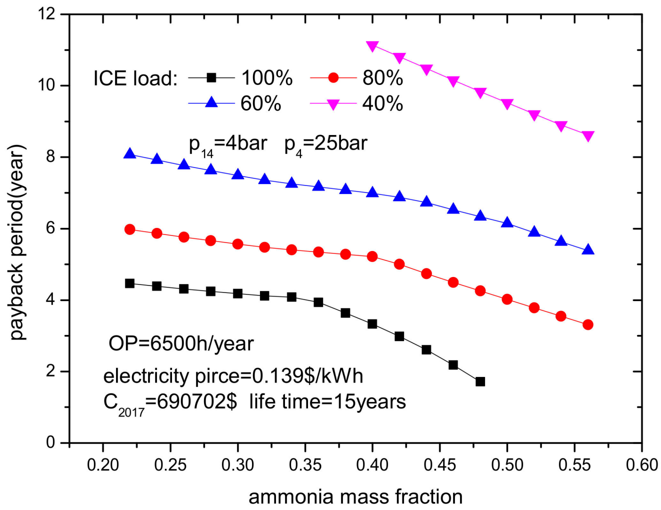


**Figure 13.** Effects of ammonia mass fraction on payback period.

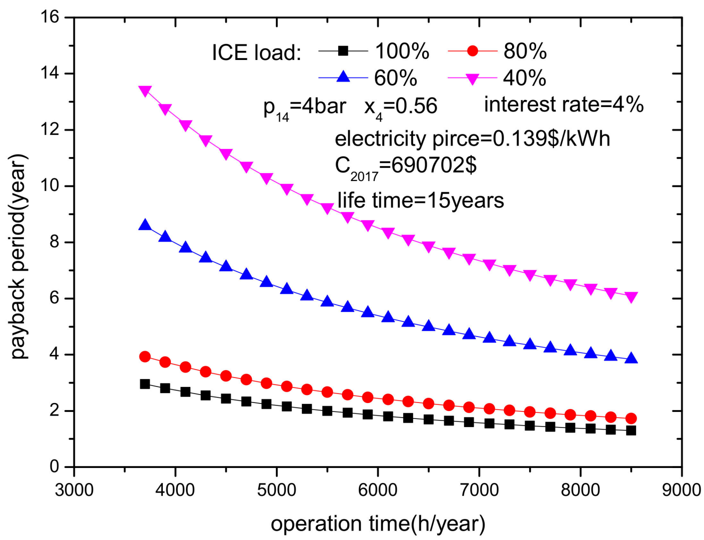


**Figure 14.** Effects of annual operation time on payback period.

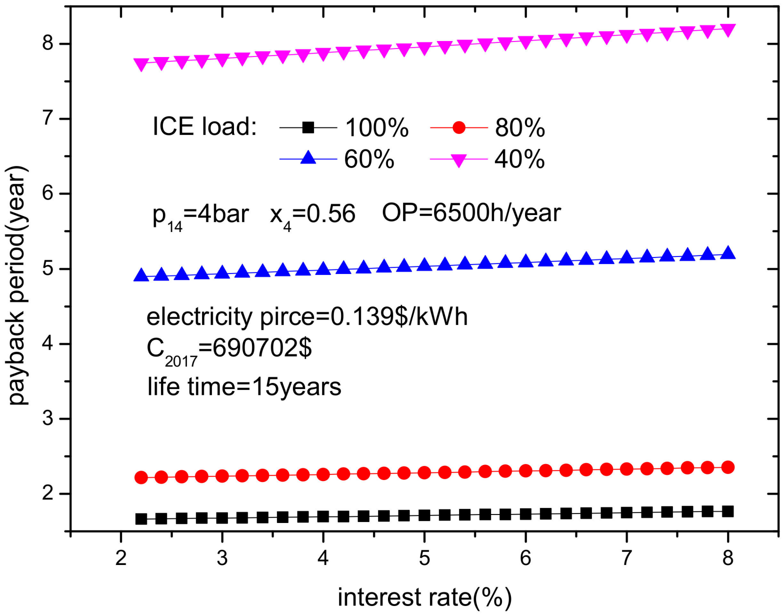


**Figure 15.** Effects of interest rate on payback period.

## 5. Conclusions

In this paper, a Kalina cycle (KC) with a superheater is used as a bottoming cycle to recover the waste heat from an internal combustion engine (ICE). The thermodynamic and economic analyses are conducted for this bottoming KC. The following conclusions are obtained:

(1) KC with a superheater is a promising cycle for waste heat recovery from ICE. The Kalina subsystem not only yields extra power output without extra petroleum consumption but also reduces the emissions of $CO_2$. The maximum net power output and thermal efficiency of KC in this paper are greater than those in the published literature for all ICE loads, and the maximum exergy efficiency is greater than that in the published literature when the ICE load is greater than 40%.

(2) The net power output, KC thermal efficiency and the improvement of the thermal efficiency of ICE increase with ICE percentage load and ammonia mass fraction. Compared with the single ICE, the increase of thermal efficiency is approximately 21.6% at 100% ICE percentage load. In addition, within the scope of this paper, if the ammonia mass fraction is below 0.34, a higher turbine inlet pressure is better for improving thermal performance. If the ammonia mass fraction is greater than 0.34, a lower turbine inlet pressure is better.

(3) The capital investment increases with ICE load because a high ICE load results in a high heat transfer area. It is assumed that the Kalina subsystem that requires the largest investment ($C_{2017}$), is used at all ICE loads in the paper. Both higher ICE loads and higher ammonia mass fractions result in shorter payback periods. If ICE load is high, a lower turbine inlet pressure is better for reducing the payback period. In addition, both longer annual operation times and lower interest rates lead to shorter payback periods. However, it is worth noting that the payback period will be longer than the ICE lifetime if the ICE load is too low and the annual operation time is too short.

**Author Contributions:** Methodology, H.G., F.C.; software, H.G.; validation, F.C.; formal analysis, H.G., F.C.; investigation, H.G., F.C.; data curation, H.G., F.C.; writing—original draft preparation, H.G., F.C.; writing—review and editing, H.G., F.C.

**Funding:** This research received no external funding.

**Conflicts of Interest:** The authors declare that there is no conflict of interests regarding the publication of this article.

## Nomenclature

| | |
|---|---|
| $A$ | heat exchanger area ($m^2$) |
| $C$ | cost rate ($) |
| $COM$ | operating and maintenance cost |
| $CRF$ | capital recovery factor |
| $E$ | exergy (kJ/kg) |
| $h$ | enthalpy (kJ/kg) |
| $i$ | interest rate |
| $m$ | mass flow rate (kg/s) |
| $OP$ | operation hours |
| ORC | organic rankine cycle |
| $p$ | pressure (bar) |
| $P$ | net power output (W) |
| $Q$ | heat transfer rate (W) |
| $s$ | specific entropy (kJ/kg K) |
| $T$ | temperature (K) |
| $x$ | ammonia mass fraction |
| $U$ | overall heat transfer coefficient |
| $W$ | power output (W) |
| Subscripts abbreviations | |
| evp | evaporator |
| $ex$ | exergy |
| $net$ | net power output |
| ICE | international combustion engine |
| $p$ | pump |
| $s$ | isentropic |
| $sup$ | superheater |
| $t$ | thermal |
| $T$ | turbine |
| Greek symbols | |
| $\eta$ | Efficiency (%) |
| $\Delta T$ | temperature difference (K) |

## References

1. Wei, M.; Fang, J.; Ma, C.; Danish, S.N. Waste heat recovery from heavy-duty diesel engine exhaust gases by medium temperature orc system. *Sci. China Technol. Sci.* **2011**, *54*, 2746–2753. [CrossRef]
2. Zhu, S.; Deng, K.; Qu, S. Energy and exergy analyses of a bottoming Rankine cycle for engine exhaust heat recovery. *Energy* **2013**, *58*, 448–457. [CrossRef]
3. Kostowski, W.J.; Usón, S. Comparative evaluation of a natural gas expansion plant integrated with an IC engine and an organic rankine cycle. *Energy Convers. Manag.* **2013**, *75*, 509–516. [CrossRef]
4. Seyedkavoosi, S.; Javan, S.; Kota, K. Exergy-based optimization of an organic Rankine cycle (ORC) for waste heat recovery from an internal combustion engine (ICE). *Appl. Therm. Eng.* **2017**, *126*, 447–457. [CrossRef]
5. Wang, X.; Shu, G.; Tian, H.; Liu, P.; Li, X.; Jing, D. Engine working condition effects on the dynamic response of organic Rankine cycle as exhaust waste heat recovery system. *Appl. Therm. Eng.* **2017**, *123*, 670–681. [CrossRef]
6. Pili, R.; Pastrana, J.D.C.; Romagnoli, A.; Spliethoff, H.; Wieland, C. Working fluid selection and optimal power-to-weight ratio for orc in long-haul trucks. *Energy Procedia* **2017**, *129*, 754–761. [CrossRef]
7. Wang, E.; Yu, Z.; Zhang, H.; Yang, F. A regenerative supercritical-subcritical dual-loop organic Rankine cycle system for energy recovery from the waste heat of internal combustion engines. *Appl. Energy* **2017**, *190*, 574–590. [CrossRef]
8. Scaccabarozzi, R.; Tavano, M.; Invernizzi, C.M.; Martelli, E. Thermodynamic Optimization of heat recovery ORCs for heavy duty Internal Combustion Engine: Pure fluids vs. zeotropic mixtures. *Energy Procedia* **2017**, *129*, 168–175. [CrossRef]

9. Liu, P.; Shu, G.; Tian, H.; Wang, X. Engine Load Effects on the Energy and Exergy Performance of a Medium Cycle/Organic Rankine Cycle for Exhaust Waste Heat Recovery. *Entropy* **2018**, *20*, 1–23.
10. Wang, X.; Shu, G.; Tian, H.; Liu, P.; Jing, D.; Li, X. Dynamic analysis of the dual-loop Organic Rankine Cycle for waste heat recovery of a natural gas engine. *Energy Convers. Manag.* **2017**, *148*, 724–736. [CrossRef]
11. Kalina, A.I. Combined-cycle system with novel bottoming cycle. *J. Eng. Gas Turbines Power* **1984**, *106*, 737–742. [CrossRef]
12. Ibrahim, O.; Klein, S. Absorption power cycles. *Energy* **1996**, *21*, 21–27. [CrossRef]
13. Fu, W.; Zhu, J.; Zhang, W.; Lu, Z. Performance evaluation of Kalina cycle subsystem on geothermal power generation in the oilfield. *Appl. Therm. Eng.* **2013**, *54*, 497–506. [CrossRef]
14. Madhawa Hettiarachchi, H.D.; Golubovic, M.; Worek, W.M.; Ikegami, Y. The performance of the kalina cycle system 11(kcs-11) with low-temperature heat sources. *J. Energy Resour. Technol.* **2007**, *129*, 243–247. [CrossRef]
15. Singh, O.K.; Kaushik, S.C. Energy and exergy analysis and optimization of Kalina cycle coupled with a coal fired steam power plant. *Appl. Therm. Eng.* **2013**, *51*, 787–800. [CrossRef]
16. Li, S.; Dai, Y. Thermo-economic comparison of kalina and $CO_2$ transcritical power cycle for low temperature geothermal sources in China. *Appl. Therm. Eng.* **2014**, *70*, 139–152. [CrossRef]
17. Yari, M.; Mehr, A.S.; Zare, V.; Mahmoudi, S.M.S.; Rosen, M.A. Exergoeconomic comparison of TLC (trilateral rankine cycle), ORC (organic rankine cycle) and Kalina cycle using a low grade heat source. *Energy* **2015**, *83*, 712–722. [CrossRef]
18. Wang, E.; Yu, Z. A numerical analysis of a composition-adjustable Kalina cycle power plant for power generation from low-temperature geothermal sources. *Appl. Energy* **2016**, *180*, 834–848. [CrossRef]
19. Fallah, M.; Mahmoudi, S.M.S.; Yari, M.; Akbarpour Ghiasi, R. Advanced exergy analysis of the Kalina cycle applied for low temperature enhanced geothermal system. *Energy Convers. Manag.* **2016**, *108*, 190–201. [CrossRef]
20. Nemati, A.; Nami, H.; Ranjbar, F.; Yari, M. A comparative thermodynamic analysis of ORC and Kalina cycles for waste heat recovery: A case study for CGAM cogeneration system. *Case Stud. Therm. Eng.* **2017**, *9*, 1–13. [CrossRef]
21. Gharde, P.R.; Sali, N.V. Design of Kalina cycle for waste heat recovery from 1196 cc multi-cylinder petrol engine. *Int. J. Adv. Res. Sci. Eng.* **2015**, *4*, 75–84.
22. Yue, C.; Han, D.; Pu, W.; He, W. Comparative analysis of a bottoming transcritical orc and a Kalina cycle for engine exhaust heat recovery. *Energy Convers. Manag.* **2015**, *89*, 764–774. [CrossRef]
23. Xu, F.; Goswami, D.Y.; Bhagwat, S.S. A combined power/cooling cycle. *Energy* **2000**, *25*, 233–246. [CrossRef]
24. Madhawa Hettiarachchi, H.D.; Golubovic, M.; Worek, W.M.; Ikegami, Y. Optimum design criteria for an organic Rankine cycle using low-temperature geothermal heat sources. *Energy* **2007**, *32*, 1698–1706. [CrossRef]
25. Zhang, S.; Wang, H.; Guo, T. Performance comparison and parametric optimization of subcritical Organic Rankine Cycle (ORC) and transcritical power cycle system for low-temperature geothermal power generation. *Appl. Energy* **2011**, *88*, 2740–2754. [CrossRef]
26. Zhu, Y.; Qu, W.; Yu, P. *Chemical Equipment Design Manual*; Chemical Industry Press: Beijing, China, 2005.
27. Qian, S. *Heat Exchanger Design Handbook*; Chemical Industry Press: Beijing, China, 2002.
28. Rodríguez, C.E.C.; Palacio, J.C.E.; Venturini, O.J.; Lora, E.E.S.; Cobas, V.M.; dos Santos, D.M.; Dotto, F.R.L.; Gialluca, V. Exergetic and economic analysis of Kalina cycle for low temperature geothermal sources in Brazil. *Appl. Therm. Eng.* **2013**, *52*, 109–119. [CrossRef]
29. Bahlouli, K.; Khoshbakhti Saray, R.; Sarabchi, N. Parametric investigation and thermo-economic multi-objective optimization of an ammonia–water power/cooling cycle coupled with an HCCI (homogeneous charge compression ignition) engine. *Energy* **2015**, *86*, 672–684. [CrossRef]
30. Xia, J.; Wang, J.; Lou, J.; Zhao, P.; Dai, Y. Thermo-economic analysis and optimization of a combined cooling and power (CCP) system for engine waste heat recovery. *Energy Convers. Manag.* **2016**, *128*, 303–316. [CrossRef]
31. Chemical Enineering. Available online: http://www.chemengonline.com/cepci-updates-january-2018-prelim-and-december-2017-final/ (accessed on 24 March 2018).
32. Chen, Y.; Han, W.; Jin, H. Investigation of an ammonia-water combined power and cooling system driven by the jacket water and exhaust gas heat of an Internal combustion engine. *Int. J. Refrig.* **2017**, *82*, 174–188. [CrossRef]
33. Wang, X.Q.; Li, X.P.; Li, Y.R.; Wu, C.M. Payback period estimation and parameter optimization of subcritical organic Rankine cycle system for waste heat recovery. *Energy* **2015**, *88*, 734–745. [CrossRef]

34. State Grid. Available online: http://www.95598.cn/person/sas/es/expenses.jsp?partNo=PM06003001 (accessed on 30 August 2018).
35. De Oliveira Neto, R.; Sotomonte, C.A.R.; Coronado, C.J.; Nascimento, M.A. Technical and economic analyses of waste heat energy recovery from internal combustion engines by the Organic Rankine Cycle. *Energy Convers. Manag.* **2016**, *129*, 168–179. [CrossRef]
36. Yamaguchi, H.; Zhang, X.R.; Fujima, K.; Enomoto, M.; Sawada, N. Solar energy powered Rankine cycle using supercritical $CO_2$. *Appl. Therm. Eng.* **2006**, *26*, 2345–2354. [CrossRef]